Materials Research Proceedings 33 (2023) 301-308 https://doi.org/10.21741/9781644902677-44

Structural modeling of manufacture-induced gaps and overlaps by high-order unified finite elements

Alberto Racionero Sánchez-Majano[1,a *]

[1]Politecnico di Torino, Corso Duca degli Abruzzi, 10129, Turin, Italy

[a,]alberto.racionero@polito.it

Keywords: Variable Angle Tow Composites, Defect Modeling, Gaps and Overlaps, Unified Formulation

Abstract. Variable stiffness composites present additional tailoring capabilities if compared to classical straight fiber composites. However, the fabrication of these advanced composites leads inevitably to the presence of manufacturing signatures such as gaps and overlaps, which alter the mechanical behavior of the laminated components. In this work, the fundamental frequency of variable stiffness laminates with the presence of gaps and overlaps is studied. The Defect Layer Method is considered for modeling the defects, while the Carrera Unified Formulation is employed to derive the governing equations which will be solved by the Finite Element Method.

Introduction

Novel manufacturing techniques, such as Automated Fiber Placement (AFP), have permitted to conceive new families of laminated structures, namely Variable Stiffness Composites (VSC) or Variable Angle Tow (VAT), in which fiber tows are steered conforming curvilinear paths. For instance, Olmedo and Gürdal [1] investigated the buckling of VAT plates for different boundary conditions and rotations of the fiber path. They conducted a parametric analysis of how the fiber path parameters affect the non-dimensional buckling load factor. They found improvements up to 19 and 80% with respect to classic laminates. However, in the cases that Olmedo and Gürdal considered, the minimum turning radius, which determines whether a laminate is manufacturable or not, was not taken into account. Therefore, not all the solutions were feasible from a fabrication point of view. Besides, due to the manufacturing features inherent to AFP, imperfections are prone to arise during the fabrication process, namely gaps and/or overlaps, and affect the structural performance [2].

Many authors have proposed numerical methods to investigate the effect of gaps and/or overlaps on the mechanical properties of variable stiffness composites. Blom et al. [2] investigated how gaps affect the strength and stiffness of VAT using the Finite Element Method (FEM). They concluded that increasing the laminate's total gap area deteriorates strength and stiffness. The main drawback of their proposed method was that a very fine mesh was required to capture the gap areas, drastically increasing the computational cost. Fayazbakhsh et al. [3] proposed the Defect Layer Method (DLM), which permits to capture the gap and/or overlap areas that appear in the laminate without incurring into an excessive computational burden as in [2].

In this manuscript, we tackle the influence of gaps and overlaps on VAT laminates by coupling DLM with the Carrera Unified Formulation (CUF) [4]. CUF permits obtaining the governing equations of any structural theory without making *ad hoc* assumptions. So far, CUF has proven to predict accurate stress states [5], as well as capture the influence of multiscale uncertainty defects on the mechanical performance of VAT plates [6].

Variable stiffness composite plates and defect modeling

VAT laminated components are fabricated by steering fiber bands along curvilinear paths. Throughout the years, different variation laws have been investigated. However, two kinds of

Materials Research Proceedings 33 (2023) 301-308 https://doi.org/10.21741/9781644902677-44

variations have been the most researched: the constant curvature and linear variation. This work focuses on the latter, in which the local fiber orientation, $\boldsymbol{\theta}$, varies along the $\boldsymbol{x'}$ direction as follows:

$$\theta(x') = \phi + T_0 + \frac{T_1 - T_0}{d}|x'|. \quad (1)$$

In the previous equation, T_0 is the fiber angle orientation at $x' = 0$, whereas the fiber angle orientation T_1 is reached at $x' = d$, being d the semi-length or semi-width of the laminate. Last, ϕ is the fiber angle path rotation, which generally equals 0° or 90°. All of these parameters are illustrated in Figure 1.

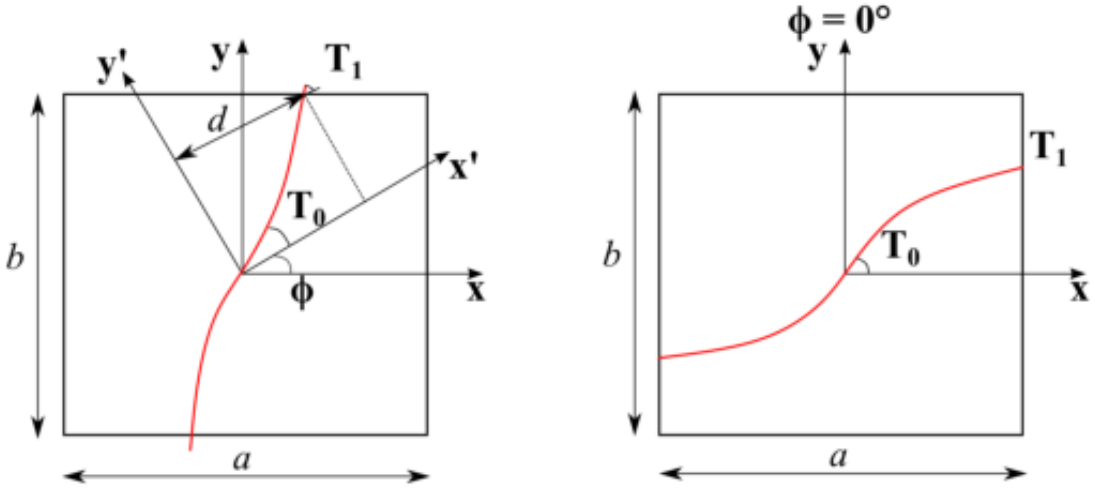

Figure 1. Representation of the fiber parameters involved in the definition of a VAT laminate.

Despite the steering capability of VAT plates, the AFP machines that manufacture them present some limitations, being one of them the curvature of the laid fiber path. In case of exceeding the turning radius, fiber wrinkles and upfolding will generate within the placed tape. An additional manufacturing feature inherent to AFP is the presence of gaps and overlaps in the final part, thereby affecting the structural performance. For instance, gaps reduce the laminate strength, while overlaps can cause an increase in strength. DLM [3] is considered to model these imperfections. As mentioned in [3], the defect area percentage is the only parameter to modify the elastic properties or the thickness associated to the finite element. Note that the elastic properties vary if gaps are considered, whereas an increase in the thickness is provided in the case of overlap. The elastic properties are modified according to Fig. 6 from [3]. The thickness increases proportionally to the defect area within the element and is topped up by 95% of the original thickness of the ply due to the compaction pressure in the autoclave, as reported in [7].

Unified finite elements

2D FE are implemented within the CUF formalism. According to [4], the 3D field of displacement can be expressed in terms of arbitrary through-the-thickness expansion functions, $\boldsymbol{F_\tau(z)}$, of the 2D generalized unknowns laying over the $\boldsymbol{x - y}$ plane. That is,

$$\boldsymbol{u}(x, y, z) = F_\tau(z)\boldsymbol{u}_\tau(x, y).\ \tau = 1, \dots, M \quad (2)$$

Therein, M denotes the number of expansion terms, and $\boldsymbol{u}_\tau(x, y)$ is the vector containing the generalized displacements. Note that τ denotes summation. The analysis of multi-layered structures is commonly conducted by following an Equivalent-Single-Layer (ESL) and Layer-Wise (LW) approach. In this manuscript, ESL models are built using Taylor polynomials as F_τ in the thickness direction. On the other hand, LW utilizes Lagrange polynomials over the single

Materials Research Proceedings 33 (2023) 301-308 https://doi.org/10.21741/9781644902677-44

layers and then imposes the continuity of displacements at the layer interfaces, as in [8]. In this context, TEn denotes a TE of the n-th order, whilst LEn indicates the usage of an LE with n-th order polynomials. Moreover, XLEn means that X Lagrange polynomials of n-th order are used to describe each layer of the laminate.

Utilizing the FE and shape functions $N_i(x, y)$, the displacement field becomes:

$$\boldsymbol{u}(x, y, z) = N_i(x, y)F_\tau(z)\boldsymbol{q}_{\tau i}(x, y).\ i = 1, \dots, N_n \tag{3}$$

In Eq. (3), $\boldsymbol{q}_{\tau i}$ denotes the unknown nodal variables, and N_n indicates the number of nodes per element. In this work, 2D nine-node quadratic elements, referred to as Q9, are employed as N_i for the $x - y$ plane discretization.

The governing equations are obtained by means of the Principle of Virtual Displacements (PVD). PVD states that the virtual variation of the internal strain energy, $\delta\mathcal{L}_{int}$, has to be equal to the virtual work of the external forces, $\delta\mathcal{L}_{ext}$, minus that of the inertia forces, $\delta\mathcal{L}_{ine}$. That is:

$$\delta\mathcal{L}_{int} = \delta\mathcal{L}_{ext} - \delta\mathcal{L}_{ine}. \tag{4}$$

In the case of free vibration analyses, Eq. (4) becomes:

$$\delta\mathcal{L}_{int} + \delta\mathcal{L}_{ine} = 0. \tag{5}$$

The virtual variation of the strain energy can be calculated as:

$$\delta\mathcal{L}_{int} = \int_V \delta\boldsymbol{\varepsilon}^{\boldsymbol{T}}\boldsymbol{\sigma}dV, \tag{6}$$

whereas the virtual work of the inertia forces is computed as:

$$\delta\mathcal{L}_{ine} = \int_V \rho\delta\boldsymbol{u}^{\boldsymbol{T}}\ddot{\boldsymbol{u}}dV, \tag{7}$$

in which ρ represents of the mass density of the material. Equation (6) can be rewritten using Eq. (3), the constitutive law $\boldsymbol{\sigma} = \boldsymbol{C\varepsilon}$, and the geometrical relations between the strains and displacements, yielding:

$$\delta\mathcal{L}_{int} = \delta\boldsymbol{q}_{sj}^T\left[\int_V \boldsymbol{D}^T(N_jF_s)\,\widetilde{\boldsymbol{C}}\boldsymbol{D}(N_iF_\tau)\,dV\right]\boldsymbol{q}_{\tau i} = \delta\boldsymbol{q}_{sj}^T\boldsymbol{k}_0^{ij\tau s}\boldsymbol{q}_{\tau i}, \tag{8}$$

where $\boldsymbol{k}_0^{ij\tau s}$ is the 3×3 Fundamental Nucleus (FN) of the stiffness matrix, which is invariant regardless of the order of the 2D shape function and the through-the-thickness expansion. $\boldsymbol{D}(\cdot)$ denotes the differential operator matrix containing the geometrical relations, and $\widetilde{\boldsymbol{C}}$ is the material stiffness matrix in the global reference frame, i.e., $\widetilde{\boldsymbol{C}} = \boldsymbol{T}(x, y)^T\boldsymbol{CT}(x, y)$. Since the fiber varies point-wise within the $x - y$ plane, so does the rotation matrix $\boldsymbol{T}$.

The virtual work of the inertia forces can be expressed as:

$$\delta\mathcal{L}_{ine} = \delta\boldsymbol{q}_{sj}^T\left[\int_V \rho\boldsymbol{I}N_iN_jF_\tau F_s\,dV\right]\ddot{\boldsymbol{q}}_{\tau i} = \delta\boldsymbol{q}_{sj}^T\boldsymbol{m}^{ij\tau s}\ddot{\boldsymbol{q}}_{\tau i}, \tag{9}$$

in which $\boldsymbol{I}$ is the 3×3 identity matrix and $\boldsymbol{m}^{ij\tau s}$ is the 3×3 FN of the mass matrix. Hence, the undamped free vibration problem can be written as follows:

Materials Research Proceedings 33 (2023) 301-308 https://doi.org/10.21741/9781644902677-44

$$\boldsymbol{M}\ddot{\boldsymbol{q}} + \boldsymbol{K_0 q} = 0. \tag{10}$$

In Eq. (10), $\boldsymbol{M}$ and $\boldsymbol{K_o}$ denote the overall mass and stiffness matrices, respectively. They are obtained by looping over the FN's through the indices i, j, τ and s to obtain the mass and stiffness matrices for the single element, and subsequently assembled to conform that of the whole structure. Last, by imposing harmonic solutions $\boldsymbol{q} = \tilde{\boldsymbol{q}}e^{i\omega t}$, Eq. (10) turns into the following eigenvalue problem:

$$(\boldsymbol{K_0} - \omega_i^2 \boldsymbol{M})\tilde{\boldsymbol{q}_i} = 0 \tag{11}$$

where ω_i and $\tilde{\boldsymbol{q}_i}$ are the i^{th} natural frequency and eigenvector, respectively.

Machine simulation: identification of gap and overlap locations.
The steering of fiber bands along a fixed direction, and shifting the AFP head in its perpendicular direction to generate the subsequent fiber course, leads to the presence of gaps and/or overlaps. The location in which they appear depends not only on T_0 and T_1 but also on the steering strategy. That is, one can impose contact between two adjacent courses at the edge or the center of the plate. Figure 2 illustrates the case of a $[\langle 0,45 \rangle]$ plate in which the fiber courses touch each other at the edge (Figure 2 left) and at the center of the plate (Figure 2 right). The yellow area indicates a gap area, whereas the green area highlights an overlap area.

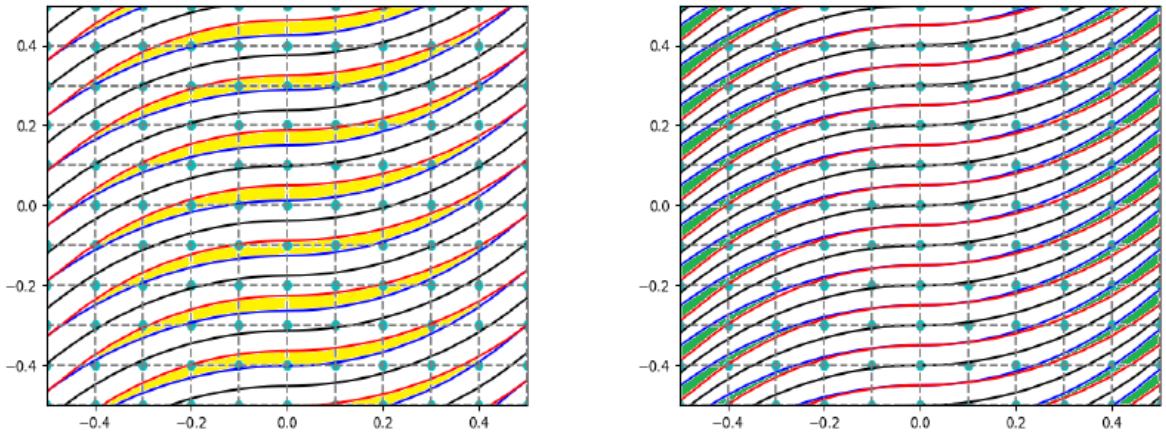

Figure 2. Example of a plate with $[\langle \mathbf{0}, \mathbf{45} \rangle]$ *stacking sequence with full gap (left) and full overlap (right) manufacturing strategy.*

Table 1 reflects the kind of defects that will arise depending on the fiber path parameters and the contact position of adjacent courses.

Condition	Contact at edge	Contact at center
$\lvert\cos T_0\rvert > \lvert\cos T_1\rvert$	Gap at center	Overlap at edges
$\lvert\cos T_1\rvert > \lvert\cos T_0\rvert$	Overlap at center	Gap at edges

Table 1. Defects arising within the plate depending on the fiber parameters and the manufacturing strategy.

The previous imperfections affect such large areas because the course width is kept constant throughout the steering process. In order to reduce the defect area, the course width has to decrease or increase whenever a course intersects the successive one or it does not reach the precedent course's edge, respectively. The increase or decrease of the course width is achieved by cutting an individual tow and restarting its deposition. This comports the generation of small triangular defected regions, as evidenced in Figure 3.

Materials Research Proceedings 33 (2023) 301-308 https://doi.org/10.21741/9781644902677-44

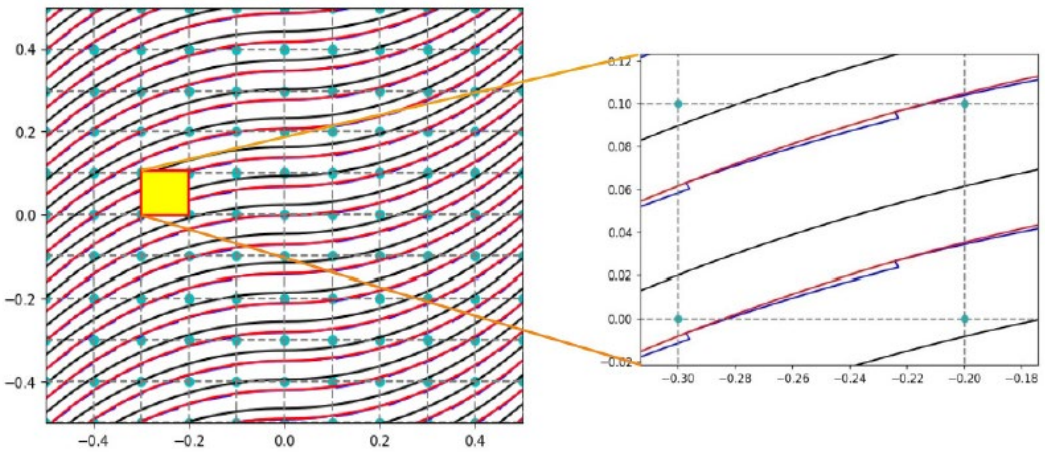

Figure 3. Gap defect correction over a $[\langle \mathbf{0}, \mathbf{45} \rangle]$ *ply The zoomed area shows the triangular gaps that are generated.*

As stated in Section 2, the material elastic properties, or element thickness, will be modified according to the defect area within each finite element.

Results

Model verification

The first step towards the maximization of the fundamental frequency of a VAT plate is the model verification. For doing so, the results presented in the work by Akhavan and Ribeiro [9] are used. A three-layered square plate with lamination sequence $[\langle \mathbf{0}, \mathbf{45} \rangle, \langle -\mathbf{45}, -\mathbf{60} \rangle, \langle \mathbf{0}, \mathbf{45} \rangle]$ is considered. The length and width of the plate are $\boldsymbol{a} = \boldsymbol{b} = \mathbf{1}$ m, and the width-to-thickness ratio is $\boldsymbol{a}/\boldsymbol{h} = \mathbf{10}$, having each ply the same thickness. The plate is clamped on all of its four edges.

First, a convergence analysis is performed employing Q9 FE and LE2 expansion through the thickness direction. The results are enlisted in Table 2. It is observed a good agreement between Ref. [9] and the present approach. Plus, convergence is reached with the 10x10 Q9 mesh, since the relative error between the 10x10 and 12x12 mesh is about 0.1%. Thus, the 10x10 Q9 mesh will be used in the upcoming analyses.

Table 2. Mesh convergence in terms of the first five fundamental frequencies of the $[\langle \mathbf{0}, \mathbf{45} \rangle, \langle -\mathbf{45}, -\mathbf{60} \rangle, \langle \mathbf{0}, \mathbf{45} \rangle]$ *plate. Each discretization uses 1 LE2 expansion per layer through the thickness direction.*

Model	DOF	f_1 [Hz]	f_2 [Hz]	f_3 [Hz]	f_4 [Hz]	f_5 [Hz]
Ref.	-	613.79	909.04	1231.65	1337.69	1484.53
6x6 Q9	3549	614.82	916.05	1230.29	1361.72	1492.04
8x8 Q9	6069	611.26	907.03	1219.97	1337.03	1475.20
10x10 Q9	9261	609.91	903.93	1216.18	1328.88	1469.58
12x12 Q9	13125	609.28	902.56	1214.47	1325.46	1467.15

Subsequently, the effect of the structural theory on the fundamental frequency is addressed. The results are available in Table 3.

Materials Research Proceedings 33 (2023) 301-308 https://doi.org/10.21741/9781644902677-44

Table 3. Effect of the structural theory on the first five natural frequencies for the $[\langle \mathbf{0}, \mathbf{45} \rangle, \langle -\mathbf{45}, -\mathbf{60} \rangle, \langle \mathbf{0}, \mathbf{45} \rangle]$ *plate. Each model employs a 10x10 Q9 mesh.*

Model	DOF	f_1 [Hz]	f_2 [Hz]	f_3 [Hz]	f_4 [Hz]	f_5 [Hz]
Ref.	-	613.79	909.04	1231.65	1337.69	1484.53
TE 1	2646	638.87	955.51	1278.43	1419.71	1553.57
TE 3	5292	611.17	908.11	1218.00	1338.39	1473.10
TE 6	9261	609.49	903.63	1214.24	1328.59	1774.46
1 LE1	5292	621.64	917.66	1244.85	1347.15	1499.66
1 LE 2	9261	609.91	903.93	1216.18	1328.88	1469.58

As expected, TE 1 model provided a higher value of f_1 since it leads to a higher stiffness of the model, whereas the TE 3 provides practically the same value of the reference, where a third-order structural theory was employed. TE 6 calculated a value very similar to 1 LE2, with the exception of the fifth fundamental frequency, where TE 6 provided a higher value. Then, regarding the LW models, the 1 LE1 approach led to the computation of fundamental frequencies that lay between those computed with a TE 3 and 1 LE2 model.

Effect of manufacturing defects: gaps and overlaps

In this section, the effect of manufacturing defects is addressed. As depicted in Section 4, two manufacturing strategies are considered: without and with defect correction. These two strategies are denoted as Type 1 and Type 2, respectively. For the following analyses, the tow paths are conformed by sixteen tows, each with a width of $t_w = 3.125$ mm. The FE mesh comprises 10x10 Q9 elements, as it showed to provide convergence in the previous subsection.

Table 4 presents the effect of gaps on the first five fundamental frequencies of the $[\langle 0{,}45 \rangle, \langle -45, -60 \rangle, \langle 0{,}45 \rangle]$ plate. An LW-1 LE2 model is employed since, when gaps are considered, the thickness of the laminate remains unaltered, and no additional computational effort is required when compared to the ideal plate. It is observed that gaps lead to a decrease in the fundamental frequency because resin-rich areas are present within the layers. Type 1 defects present a much lower frequency than the ideal case, whereas Type 2 limits the fundamental frequency reduction.

Table 4. Effect of manufacturing gaps on the $[\langle \mathbf{0}, \mathbf{45} \rangle, \langle -\mathbf{45}, -\mathbf{60} \rangle, \langle \mathbf{0}, \mathbf{45} \rangle]$ *plate. Each model uses a 10x10 Q9 mesh and 1 LE2 structural theory.*

Model	f_1 [Hz]	f_2 [Hz]	f_3 [Hz]	f_4 [Hz]	f_5 [Hz]
No defects	609.91	903.93	1216.18	1328.88	1469.58
Gap Type 1	547.82	797.10	1083.41	1159.71	1295.57
Gap Type 2	599.10	888.99	1193.21	1306.87	1442.75

The influence of overlap imperfections is gathered in Table 5. An LW-1 LE2 and ESL-TE 3 were considered for the ideal case, whereas only an ESL-TE 3 expansion is considered when modeling overlaps. As expected, the overlaps stiffen the structure, which leads to higher fundamental frequencies. Therefore, overlap Type 1 provides higher frequencies than Type 2, in which defects are reduced by modifying the number of tows while steering them.

An ESL approach is utilized when overlaps are involved due to the vast increase in terms of DOF that an eventual LW model may lead to. In an overlap LW model, the continuity of the interfaces has to be guaranteed through the thickness but also within the ply. In this regard, the number of DOF dramatically increases for a minimal improvement in the prediction of the fundamental frequency.

Table 5. Effect of manufacturing overlaps on the $[\langle \mathbf{0}, \mathbf{45} \rangle, \langle -\mathbf{45}, -\mathbf{60} \rangle, \langle \mathbf{0}, \mathbf{45} \rangle]$ *plate. Each model uses a 10x10 Q9 mesh and the Overlap Types use a TE 3 structural theory.*

Model	f_1 [Hz]	f_2 [Hz]	f_3 [Hz]	f_4 [Hz]	f_5 [Hz]
No defects 1 LE2	609.91	903.93	1216.18	1328.88	1469.58
No defects TE 3	611.17	908.11	1218.00	1338.39	1473.10
Overlap Type 1	679.02	980.20	1290.34	1414.51	1558.46
Overlap Type 2	620.72	922.19	1230.51	1356.06	1490.76

Conclusions

This manuscript has discussed the effect of manufacture-induced gaps and overlaps on the fundamental frequency of VSC laminates. First, ideal VAT plates have been modeled using CUF-based FE, and have proven to provide similar results as those found in the literature. Later, the position where gaps and overlaps will appear during manufacturing has been predicted. These defects were incorporated into the FE model by means of the Defect Layer Method. The presence of gaps incurred a decrease in the fundamental frequency, whereas overlaps led to an increase of it due to the stiffening effect they have on the structure.

Future works will be related to the optimization of VAT plates in which the aforementioned manufacturing imperfections are considered.

Acknowledgements

This work is part of a project that has received funding from the European Research Council (ERC) under the European Union's Horizon 2020 research and innovation programme (Grant agreement No. 850437). The author would also like to thank Eugenio Sabatini for providing some of the results shown in this document.

References

[1] R. Olmedo, Z. Gürdal. Buckling response of laminates with spatially varying fiber orientations. In 34th Structures, Structural Dynamics and Materials Conferences (1993), 1567. https://doi.org/10.2514/6.1993-1567

[2] A.W. Blom, C.S. Lopes, P.J. Kromwijk, Z. Gürdal, P.P. Camanho. A theoretical model to study the influence of tow-drop areas on the stiffness and strength of variable-stiffness laminates. Journal of Composite Materials 43(5) (2009), 403-425. https://doi.org/10.1177/0021998308097675

[3] K. Fayazbakhsh, M.A. Nik, D. Pasini, L. Lessard. Defect layer method to capture effect of gaps and overlaps in variable stiffness laminates made by automated fiber placement. Composite Structure 97 (2013), 245-251. https://doi.org/10.1016/j.compstruct.2012.10.031

[4] E. Carrera, M. Cinefra, M. Petrolo, E. Zappino. Finite Element Analysis of Structures through Unified Formulation. Wiley & Sons, Hoboken, New Jersey. 2014.

[5] A.R. Sánchez-Majano, R. Azzara, A. Pagani, E. Carrera. Accurate stress analysis of variable angle tow shells by high-order equivalent-single-layer and layer-wise finite element models. Materials 14(21) (2021), 6486. https://doi.org/10.3390/ma14216486

[6] A. Pagani, M. Petrolo, A.R. Sánchez-Majano. Stochastic characterization of multiscale material uncertainties on the fibre-matrix interface stress state composite variable stiffness plates.

International Journal of Engineering Science 183 (2023), 103787. https://doi.org/10.1016/j.ijengsci.2022.103787

[7] A.A. Vijayachandran, P. Davidson, A.M. Waas. Optimal fiber paths for robotically manufactured composite structural panels. International Journal of Non-Linear Mechanics 126 (2020), 103567. https://doi.org/10.1016/j.ijnonlinmec.2020.103567

[8] E. Carrera. Theories and finite elements for multi-layered, anisotropic, composite plates and shells. Archives of Computational Methods in Engineering 9(2) (2002), 87-140.

[9] H. Akhavan, P. Ribeiro. Natural modes of vibration of variable stiffness composite laminates with curvilinear fibers. Composite Structures 93(11) (2011), 3040-3047. https://doi.org/10.1016/j.compstruct.2011.04.027